

Bubble and Temperature Fields in Langmuir Circulation

David Farmer¹, Svein Vagle¹ and Ming Li¹

¹Institute of Ocean Sciences, 9860 West Saanich Road, Sidney, BC, V8L 4B2
Canada

Abstract. Observations of temperature variability and bubble distributions during a storm illustrate aspects of Langmuir circulation relevant to vertical exchange processes in the upper ocean. During the early part of the storm, fine scale temperature measurements reveal vertically coherent structure throughout the mixing layer, with cold plumes descending from the cooling air-sea interface, separated by rising warmer water. Bubbles penetrate to greater depths in the cooler water, consistent with an interpretation of organization of the bubbles by active Langmuir circulation. However, a two-dimensional scaling leads to scattered results suggesting that other effects, such as entrainment of higher salinity water at the base of the active mixing layer, may also be important. Measurements of bubble size distributions are used to calculate averaged horizontal buoyancy gradients which are greater than thermal effects but small compared to the wave-shear interaction. During the latter part of the storm, vertical coherence of the temperature field breaks down, an effect which is also coincident with rapid deepening of the mixed layer.

1 Introduction

Langmuir circulation is a key process contributing to turbulent mixing in the upper ocean boundary layer. The mixing differs qualitatively from diffusion due to small scale turbulence, since the vertical scale of Langmuir cells can be comparable to the depth of the layer that is being actively mixed by the wind, ensuring rapid redistribution of heat and other properties transferred through the air sea interface. Due to its coherent structure, Langmuir circulation does not simply mix heat or other properties uniformly through the water column, but instead generates discernible property contrasts between upwelling and downwelling plumes. Fine scale temperature variability in the upper ocean is easily measured and may therefore serve as a tracer of upper ocean turbulent flows influencing mixed layer deepening. It is possible, for example, that horizontal temperature variability is related to the process of vertical entrainment whereby Langmuir circulation breaks down pre-existing vertical stratification and entrains water from greater depths [1]. The potential for measuring such processes provides motivation for understanding the origin and behavior of small scale thermal structure in the upper ocean.

Bubbles are created by breaking waves and occur near the ocean surface whenever the wind rises above $\sim 5\text{ms}^{-1}$. Wind generated bubble clouds therefore normally coexist with Langmuir circulation which tends to organize

them into elongated structures that are oriented in the general direction of the wind. Bubbles are readily detected by acoustical means and therefore also trace water motion and mixing. However the character of bubbles as tracers of upper ocean circulation is fundamentally different from that of thermal structure because bubble populations are not a conservative property but tend to be lost due to dissolution and buoyancy. This accounts for the fact that bubbles tend to be confined to the top few meters of the ocean, whereas temperature structure associated with wind driven mixing can extend throughout the active mixing layer. Here we describe observations of both bubbles and fine scale temperature anomalies in the upper ocean and show how they are related to the circulation. It has been suggested that the buoyancy associated with bubbles could have dynamical significance. We take the opportunity provided by simultaneous measurements of both the bubbles and temperature anomalies to calculate their potential influence on Langmuir circulation.

Langmuir circulation was first described half a century ago [2], but a firm fluid dynamical interpretation had to wait for the seminal contributions of Leibovich and his co-workers [3,4,5,6]. The Craik-Leibovich model (CL) is now widely accepted as an explanation for the generation of vortical motions extending over the depth of the layer that is being actively mixed, which are characteristic of the wind driven upper ocean boundary layer. The application of modern measurement techniques to the study of Langmuir circulation is relatively recent. Measurements of turbulence, ocean surface temperature variability, acoustic imaging, acoustic Doppler profiling and the tracking of neutrally buoyant floats [7], are now starting to fill in the record. At the same time innovative new modeling techniques, including large eddy simulations, are being applied to upper ocean circulation [8,9]. Here we describe open ocean observations of the fine scale temperature field and bubble size distributions, two properties which might provide focus for future model comparisons.

There have been numerous measurements of temperature variability associated with Langmuir convergence zones [10,11]. Some evidence for the coincidence of temperature anomalies with wave breaking [12] and bubble distributions [13] has also been described and comparisons made with semi-empirical models that combine organized circulation with turbulent diffusion of heat [14]. However the detailed thermal structure throughout the mixing layer remains to be described and explained. The organization of bubbles by Langmuir circulation is a prominent feature of acoustic images [15,16] and has motivated model studies of the role of bubbles in contributing to air-sea gas flux [17]. Simultaneous measurements of bubble distributions and the horizontal component of near-surface currents [18] generally support the concept of downwind jets within convergence zones while also illustrating a somewhat ambiguous relationship between the spatial structure of the bubble and velocity field. Typically, the organization of bubble clouds does not follow a linear two-dimensional cellular structure, but exhibits time

dependence and multiple branching [16]. Recent LES modeling efforts have moved beyond the two-dimensional picture of Langmuir circulation and point to a continuously evolving pattern with merging and break-up of Langmuir cells over a range of scales.

2 Observational Approach

We have used a combination of *in situ* and remote sensing methods to sample the upper ocean. In order to acquire measurements beyond the influence of a ship while at the same time sampling a drifting water body so as to observe its temporal evolution, we have used an array of internally recording instruments supported from surface buoys. Three types of observation are discussed here: temperature time series measured with a vertical array of internally recording temperature sensors, bubble radius distributions measured with a vertical array of acoustical resonators and the horizontal bubble cloud distribution imaged with a scanning sonar.

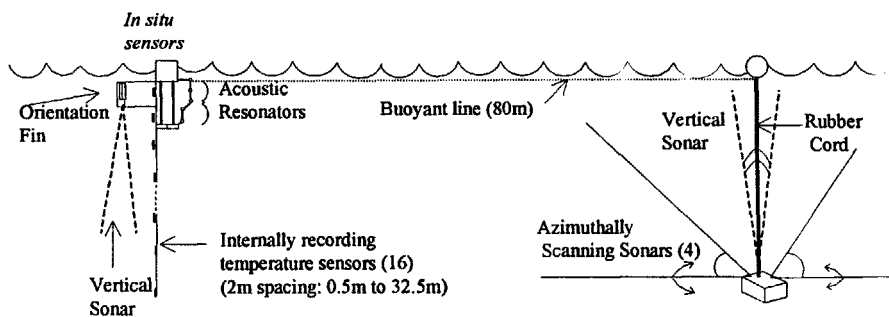


Figure 1: Sketch of deployment arrangement consisting of two tethered systems, an instrumented buoy and a subsurface sonar system. The instrumented buoy lies within the field of view of the sonars.

The deployment arrangement (Figure 1) is designed so as to ensure that measurements of the bubble size distribution and temperature structure acquired with *in situ* sensors can be placed in context with the larger scale field of organized bubble clouds and circulation. An instrumented buoy is tethered by an 80m length of floating line to a small float. Beneath this float a rubber cord suspends a horizontally imaging sonar [16] at a depth of approximately 30m. The imaging sonar consists of 4 mechanically driven

100kHz sonars that sweep azimuthally, producing a radar like image of the surface bubble clouds at intervals of approximately 30s. The subsurface system also includes a narrow beam sonar pointing vertically upwards for imaging bubble cloud penetration, similar to a downward pointing sonar mounted on the instrumented buoy. The wind driven shear and differential drag between the two drifting components ensures that the instrumented buoy lies downwind of the sonar system at a location always falling within the scanning sonar's field of view. The scanning sonar could also be programmed to acquire Doppler measurements with the beams at fixed compass headings. This arrangement allows measurement of the directional wave field [20] which may be used to calculate the Stokes drift velocity. Measurements acquired by the drifting instruments were supported by numerous density profiles, meteorological data and measurements of dissolved gases.

The temperature sensors were deployed at 17 equally spaced depths between 0.5m and 32.5m. Each sensor acquired a measurement every 5s; calibrations were carried out against a platinum thermometer and the measurements have an accuracy of 0.01°C and resolution of 0.001°C. Temperature variations relative to the mean at each depth were used to develop highly resolved images of coherent thermal structure within the layer of active mixing. A second narrow beam sonar pointing straight down is located on the buoy's orientation fin. Although acoustical scatter from the vertical instrument array causes some contamination of the signal, measurements from this sonar are useful because they provide an indication of bubble cloud penetration coincident with the local temperature measurements.

The bubble size distribution was measured from the bulk acoustical dispersion of the water using resonators [19]. Measurements of acoustic attenuation as a function of frequency can be inverted to recover the size distribution and the results checked against the measured frequency dependence of sound speed. The observations were acquired at intervals of 0.8s over a bubble size range of 15-550 μm , with up to 5 sensors at depths of 0.8m to 4.5m. Other sensors were used to sample the air entrainment within the white-cap and a vertical sonar on the same mooring measured the overall vertical distribution of bubble density.

3 Results

Our observations were made from 8 November 1977 1700h to 9 November 1200h in the open ocean, west of Vancouver Island. At 1900h on the 8th, the wind rose rapidly and maintained a speed of $U_{10} \sim 14\text{ms}^{-1}$ through 1200h on the 9th, holding a generally steady direction of 100-110°N. Towards the end of the storm, the wind mixed layer had increased in depth from 12 to 40m. The instrumentation was deployed on drifting buoys so as

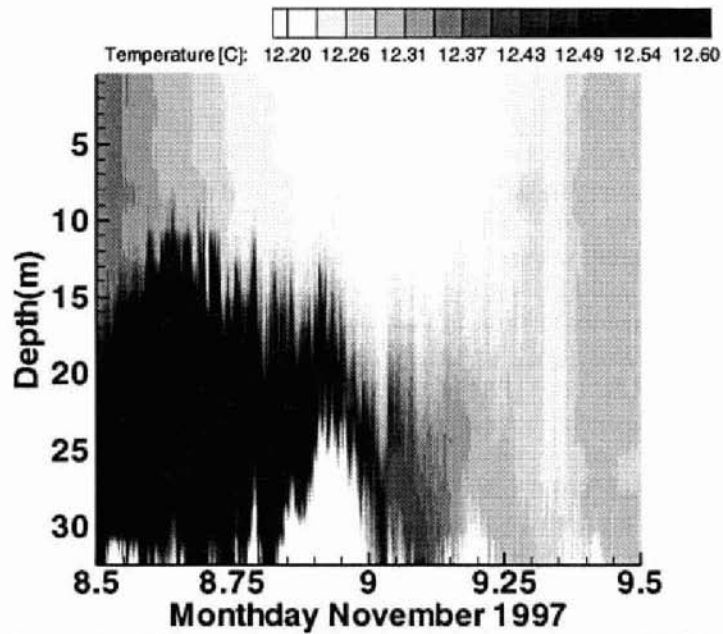


Figure 2a: Contour image of temperature over upper 32.5m during storm.

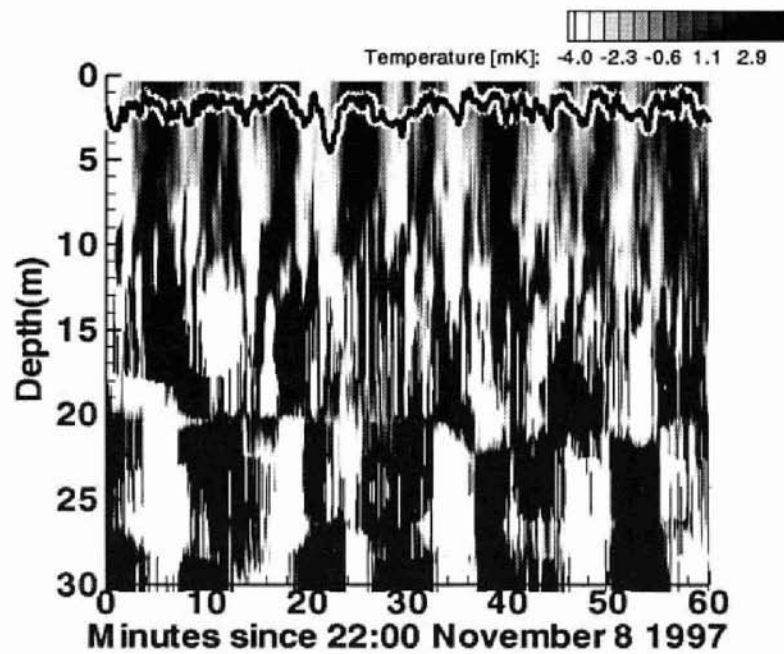


Figure 2b: Temperature deviations for a 1h period relative to the mean. The actively mixed layer extends to ~ 12 m. At top of image: a time series measurement related to bubble cloud penetration is shown. This is derived from a downwards pointing sonar and shows bubble penetration in cool (descending) water.

to follow, as far as possible, the same water mass; however, there was significant coastal influence, resulting in spatial variability of water properties.

Figure 2a shows the overall development of the temperature field through the storm. A warm layer centered at 20m is progressively eroded leading to a general warming of the surface waters, even though the ocean was losing heat at this time ($Q \sim 160 \text{Wm}^{-2}$ derived from bulk methods). The density of this warmer layer was stabilized by a 0.7psu increase in salinity. Figure 2b shows a short section of the data expanded to illustrate the fine scale variability of temperature deviations relative to the mean at each depth, revealing well developed structures penetrating through the mixing layer with amplitude of $\sim 10\text{mK}$. The cool plumes, which we identify as Langmuir convergence zones, are descending and are associated with increased bubble penetration which is shown on the same figure. The bubble penetration depth shown here is derived from the depth of a contour of constant back scatter intensity measured by the downwards pointing sonar adjacent to the thermistors. Although the intensity contour is selected so as to be always stronger than interference from the adjacent instruments and therefore understates the maximum penetration depth of bubbles, it illustrates the tendency for bubbles to collect in convergence zones. Temperature fluctuations beneath the mixed layer appear to be phase-locked to temperature variability in the mixing layer, suggesting a dynamic coupling between the Langmuir circulation and the deeper, stratified layer.

Figure 3a is a scanning image of the horizontal distribution of bubble clouds acquired from the subsurface sonar system. To some extent the appearance of bubble clouds in the image depends on the angle at which they are viewed. Close to the origin the small scale features are emphasized, while at greater ranges the cross-wind field is more sharply defined than the upwind or downwind bubble clouds. The back scatter image has a characteristic pattern indicating general alignment of the bubble clouds with the wind, although there is much variability in the structure. Time series observations from the upwards directed sonar mounted on the submerged instrument platform (Figure 3b) show that bubbles can penetrate 15-20m before dissolving.

Rapid injections of bubbles measured by our vertical resonator array have power law distributions of bubble radius with slope -2 to -2.5 over the measured range (15-550 μm), similar to observations in the surf zone [21] for bubbles of radius $< 2\text{mm}$. We attribute such injections to recent wave breaking events. This characteristic bubble field is transient, rapidly evolving under the influence of buoyancy and dissolution towards a distribution in which the volume scaled bubble spectrum has a peak at around 100 μm . The change in bubble spectrum depends on the age of the bubble cloud and its depth. The bubble clouds are drawn towards Langmuir convergence zones where the volume scaled spectral peak occurs at a progressively smaller radius with increasing depth.

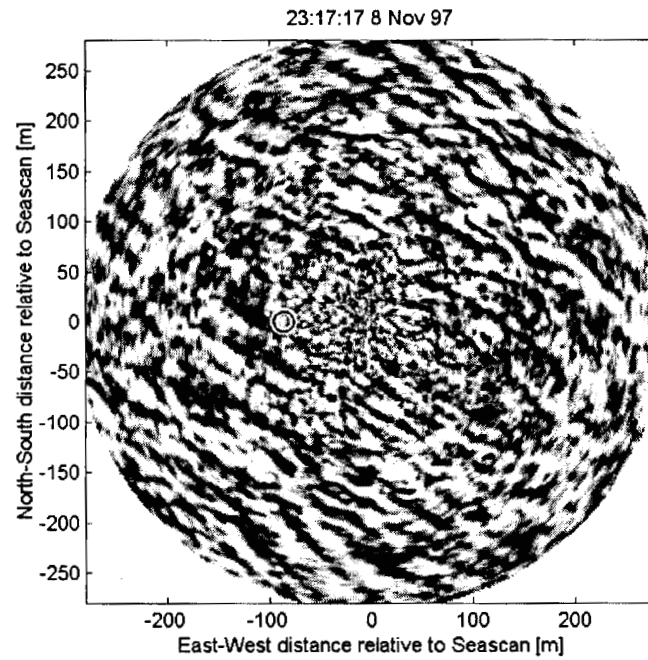


Figure 3a: Scanning sonar image showing bubble clouds along wind direction. Small circle west of center shows location of *in situ* measurement array.

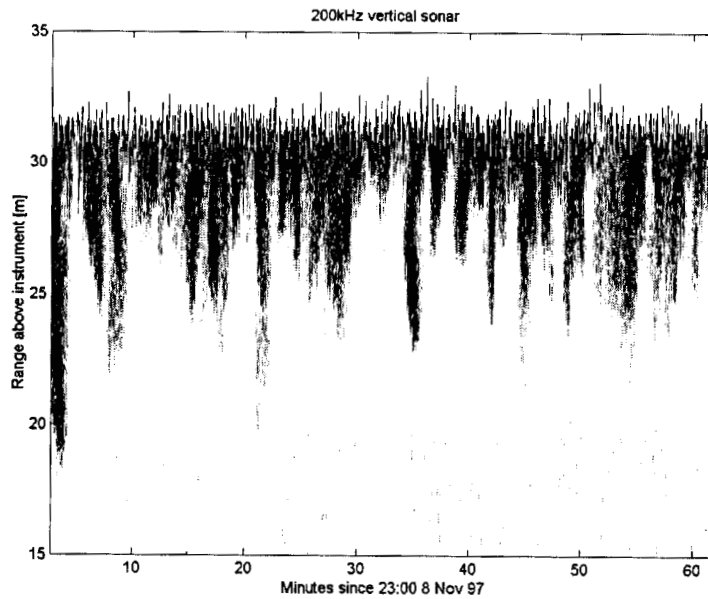


Figure 3b. Vertical sonar measurement of bubble cloud penetration.

Detailed analysis of horizontal sonar scans of the kind shown in Figure 3a, together with concurrent resonator measurements and the vertical sonar measurements made from the surface buoy, confirm that the elongated structures apparent in the sonar images such as Figure 3a are co-located with vertically penetrating bubble plumes. We therefore focus on the numbers and size distribution of bubbles at different locations within Langmuir cells. The half-width between two convergent zones was $\sim 20\text{m}$, but irregularity in the Langmuir cell structure requires that we adopt a conditional approach to sampling. From a sequential passage of well defined convergence zones we derive the average bubble conditions as a function of their position within the Langmuir cell. This sampling method collocates the dense bubble clouds from successive convergence zones, thus preserving the magnitude of contrasts in bubble concentration despite variability in the local cell spacing. Figure 4 shows the conditionally sampled air-fraction obtained by integration over the measured bubble concentration at different depths. Although much higher air-fractions occur for brief periods after a wave breaks, these are randomly distributed and contribute only to the background variability. The difference near the surface between averaged air-fraction in a convergent and divergent zone is of order 10^{-5} .

4 Discussion

Dimensional considerations based on a 2-dimensional exploration of the Craik-Leibovich model of Langmuir circulation [22] imply that the surface horizontal temperature deviation $\delta\theta$ between divergent and convergent flow depends on the surface heat flux Q and friction velocity u_* in the following way:

$$\delta\theta = c \frac{Q}{c_p \rho_w} S_0^{-\frac{1}{3}} P_r^{\frac{1}{2}} La^{-\frac{1}{6}} u_*^{-\frac{2}{3}} \quad (1)$$

where c_p is the specific heat and ρ_w the density of water, $2S_0$ is the surface Stokes velocity, P_r is the Prandtl number and La the Langmuir number. The constant c is estimated to be approximately 2. The $-1/6$ power of the Langmuir number suggests that the temperature deviation $\delta\theta$ depends only weakly on turbulence. Neglecting variations in the Prandtl and Langmuir numbers, the scaling predicts that an increasing heat flux will increase the temperature deviation while an increasing friction velocity and Stokes drift will lead to a decrease. Figure 5 shows the surface temperature anomaly $\delta\theta$. Although wind speed, wave conditions and heat flux vary only moderately during the storm (MonthDay 8.9-9.4), $\delta\theta$ varies by at least a factor of four over the same period.

The same data set is expressed in Figure 6 as a function of the dimensionless heat flux

$$H_o = \frac{g\alpha Q}{S_o\beta u_*^2} \quad (2)$$

where α is the volume coefficient of expansion and $(1/2\beta)$ is the Stokes drift e-folding depth. The points are rather narrowly clustered in heat flux but broadly scattered in temperature deviation, with no obvious trend. Assuming a Prandtl number of unity, the data imply Langmuir numbers of order 0.01 to 0.1, but the scatter suggests that other physics not included in the model, such as 3-dimensional structure, may be important.

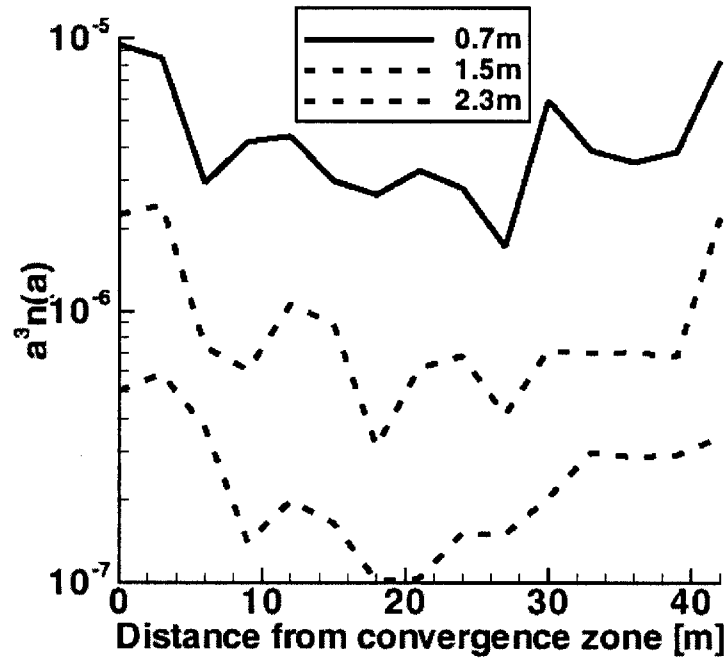


Figure 4: Conditionally averaged air-fraction due to suspended bubbles, found by integrating over measured bubbles as a function of distance from convergence zone. Based on a 1h average.

The presence of more saline water just beneath the actively mixed layer might be expected to influence the thermal structure. Examination of short period fluctuations of the salinity measured from our instrumented buoy, showed that, although exhibiting scatter the temperature variability associated with passage of Langmuir cells past the sensors was indeed correlated with salinity fluctuations. For these rapid fluctuations, a temperature-salinity analysis revealed that a 10mK increase in temperature was accompanied by a 0.013psu increase in salinity. The scaling implied by (2) does not include this effect. If we assume that the role of salinity is simply to offset the temperature anomaly associated with surface cooling,

this can be expressed by a corresponding reduction in α . This has the effect of proportionately reducing the dynamic role of the heat flux in generating vorticity and changing the magnitude of the temperature anomaly, but would not change the overall scatter. An alternative potential source of scatter is entrainment as the wind mixing layer advances into the denser and more saline water beneath.

Breakdown of the 2-dimensional structure of the circulation is also apparent in the temperature measurements. After 0700h on 9 November (MonthDay 9.3), the vertical coherence so evident in Figure 2b breaks down. One way of illustrating this is with an analysis (Fig. 7) in which the temperature variability at each depth is correlated at zero lag with the time series at 0.5m.

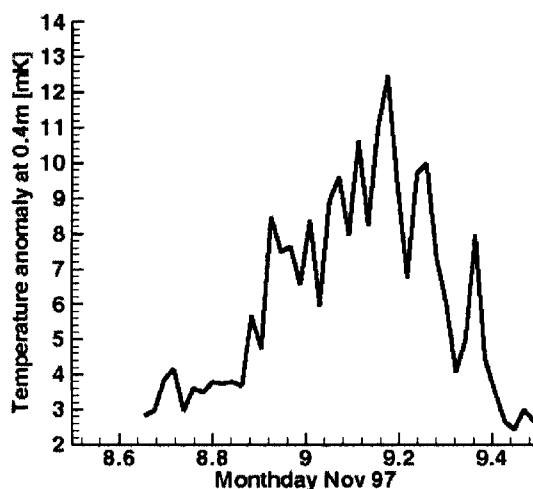


Figure 5: Measured root mean square temperature difference between divergent and convergent zones at the ocean surface as a function of time during the storm.

Between MonthDay 8.9 and 9.3 the temperature signal is highly correlated over most of the mixing layer depth, but after 0700h (MonthDay 9.3) the correlation drops to <0.3 . Wave conditions prevented acquisition of density profiles during this period, but by 1121h the mixed layer depth had increased to 40m.

Loss of coherence in the surface structure of Langmuir circulation has been described previously by Smith [18], who suggested that bubbles might play a dynamical role. Could the observed loss of coherence in the temperature field be a consequence of suppression of the Langmuir cell generation mechanism by gradients in the bubble buoyancy? The ‘Craik-Leibovich’ torque due to interaction between Stokes drift and wind shear appears as the second term on the right hand side of the equation describing the rate of change of vorticity [5] while the third term describes the contribution of the thermal anomaly:

$$\frac{\partial \Omega}{\partial t} + v \frac{\partial \Omega}{\partial y} + w \frac{\partial \Omega}{\partial z} = \nu_T \nabla^2 \Omega - \frac{du_s}{dz} \frac{du}{dy} + \tilde{\alpha} g \frac{\partial \theta}{\partial y} + g \frac{\partial A_f}{\partial y}, \quad (3)$$

where Ω is vorticity in the downwind direction, the z axis is vertical with origin at the surface, the y axis is cross-wind with origin at the location of maximum divergence, u_s is the Stokes drift, ν_T turbulent viscosity, $\tilde{\alpha}$ is the volume coefficient of expansion which could include an adjustment to accommodate salinity anomalies, g is gravity and θ temperature. We also include the contribution due to the suspended air-fraction A_f . Bubbles accumulate in convergence zones so that the resulting torque is always in opposition to the wave induced torque, whereas the thermal contribution depends on the sign of the heat flux.

We may estimate the contribution of the observed bubble distribution and temperature anomaly to the rate of change of vorticity. From Figure 4 the horizontal gradient in air fraction at the surface, between divergent and convergent zones for a separation of 20 m, gives a value of $-5 \times 10^{-6} \text{ s}^{-2}$ for the corresponding term in (3). For the observed temperature deviation between convergent and divergent zones, the corresponding temperature anomaly is of order 0.02°C , giving a contribution of $2 \times 10^{-6} \text{ s}^{-2}$ which, since the ocean is cooling, acts to increase the vorticity in opposition to the bubble effect. Thus

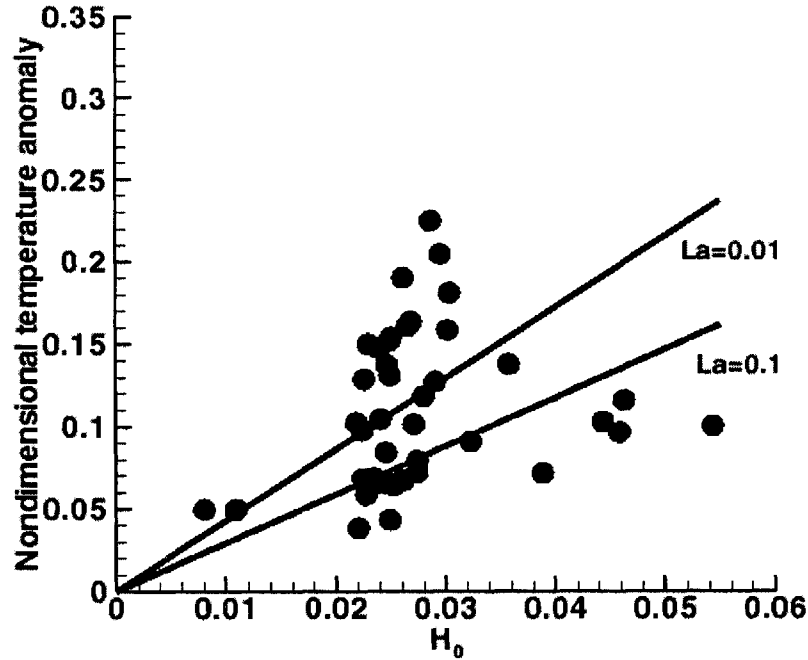


Figure 6: Dimensionless surface temperature anomaly as a function of dimensionless heat flux. Scaling based on [22]. Lines show predicted distributions for specific Langmuir numbers

the buoyancy torque due to bubbles is somewhat greater in magnitude than the thermal torque, even in the absence of salinity effects. For a Stokes drift velocity of $\sim 0.15 \text{ ms}^{-2}$ derived from the directional wave spectra and a nominal downwind jet strength of comparable magnitude [18], the wave induced contribution to vorticity change is $\sim 3.8 \times 10^{-4} \text{ s}^{-2}$. On this basis it appears that the Craik-Leibovich torque far outweighs thermal or bubble effects.

Although the buoyancy associated with a single wave-breaking event can be large, it appears that the mean buoyancy gradient is not that significant. Bubble injection and surface heat exchange contribute to the generation of mean horizontal buoyancy gradients in quite different ways. Heat is exchanged continuously across the air-sea interface leading to a progressively increasing temperature anomaly in convergence zones. The buoyancy associated with bubble injections in a divergent zone is largely lost by the time the bubble cloud remnants reach the convergent zone, due to bubbles rising to the surface as well as dissolution effects. In contrast to the effects of air-sea heat exchange, the accumulation of bubbles in the

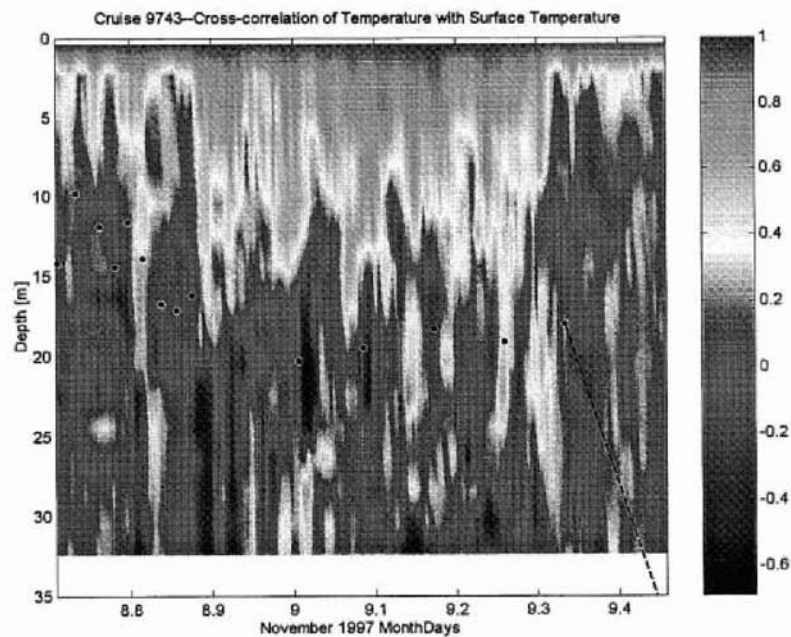


Figure 7: Correlation between surface temperature record and time series at each depth of measurement. Points show depth of mixing layer inferred from the step change in CTD density profiles. The dashed line is an interpolation over a period for which sea states were too high to permit shipboard operations.

convergent zones is primarily due to local injection rather than being due to an accumulation of injection effects throughout the surface. The results described here must be regarded as preliminary; the behavior of bubble clouds and their organization warrants further observation and analysis.

If we dismiss the buoyancy contribution of bubbles within convergence zones as a potentially disrupting influence on the Langmuir circulation, we are still left with one variable that might be relevant. During the period of low vertical coherence the mixed layer almost doubled in depth. During a period of rapid deepening it is possible that the organized behavior of Langmuir circulation becomes unstable.

5 Conclusions

Bubbles collect in convergence zones which also have anomalous temperature structure due to air-sea heat exchange. The temperature structure provides a signature of the circulation detectable throughout the mixing layer. The buoyancy gradient contribution to the rate of change of vorticity due to cooling is exceeded by an opposing effect due to the buoyancy of suspended bubble populations, but both the averaged bubble and thermal gradient effects are small compared to the wave-shear interaction. A two-dimensional model analysis fails to collapse the measured surface temperature anomalies, suggesting that three dimensional processes may be important. This possibility receives support from observations during the latter part of the storm when the mixed layer increased in thickness rapidly at the same time as vertical coherence in the temperature field was lost.

As new observations are obtained, it is to be hoped they will continue to provide sufficient fluid dynamical challenges to keep Sid Leibovich thinking about these problems for many years to come!

Acknowledgement

This work is supported by the US Office of Naval Research.

References

1. M.Li, C.Garrett (1997) Mixed Layer Deepening Due to Langmuir Circulation. *J. Phys. Oceanogr.*, Vol. 27, No. 1, 121-132
2. I. Langmuir (1938) Surface Motion of Water Induced by Wind. *Science*, 87, 119-123
3. A.D. Craik, S. Leibovich (1976), A Rational model for Langmuir Circulations. *J. Fluid Mech.*, 73, 401-426.

4. A.D.D.Craik (1977) The Generation of Langmuir circulations by an instability mechanism. *J. Fluid Mech.*, 81, 209-223
5. S.Leibovich (1977) On the evolution of the system of wind drift currents and Langmuir circulations in the ocean. Part 1. Theory and averaged current. *J. Fluid Mech.*, 79, 715-743.
6. S. Leibovich (1983) The form and dynamics of Langmuir circulations. *Annual Review of Fluid Mechanics*, 15, 391-427.
7. E.A., D'Asaro, D.M. Farmer, J. Osse, G.T. Dairiki (1996) A Lagrangian Float, *J. Oceanic & Atmosph. Tech.*, Vol.13, No.6, December, pp 1230-1246
8. E.D. Skillingstad, D.W. Denbo (1995) An Ocean Large-eddy Simulation of Langmuir Circulations and Convection in the Surface Mixed Layer. *J. Geophys. Res.* 100, 8501-8522
9. J.C. McWilliams, P.P. Sullivan, C.H. Moeng (1997) Langmuir Turbulence in the Ocean. *J. Fluid Mech.* 334, 1-30.
10. G.E. Myer, (1969) A Field Study of Langmuir Circulations. *Proceedings of the 12th Conference on Great Lakes Research*, University of Michigan, International Association for Great Lakes Research, 652-663.
11. S. A. Thorpe, A.J. Hall (1982) Observations of the Thermal Structure of Langmuir Circulation. *J. Fluid Mech.*, 114, 237-250
12. D.M. Farmer, J.R. Gemmrich (1996) Measurements of Temperature Fluctuations in Breaking Surface Waves, *J. Phys. Oceanogr.*, Vol. 26, No. 5, 816-825
13. S.A. Thorpe, A.J. Hall (1987) Bubble Clouds and Temperature Anomalies in the Upper Ocean. *Nature*, 328, 48-51.
14. J.R. Gemmrich, D.M. Farmer (1999) Near Surface Turbulence and Thermal Structure in a Wind Driven Sea, *J. Phys. Oceanogr.* , Vol. 29, No.3, 480-499
15. S.A. Thorpe (1984) The Effect of Langmuir Circulation on the Distribution of Submerged Bubbles Caused by Breaking Wind Waves. *J. Fluid Mech*, 114, 237-250.
16. D.M. Farmer, M. Li (1995) Patterns of Bubble Clouds Organized by Langmuir Circulation, *J. Phys. Oceanogr.* Vol. 25, No. 6, 1426-1440.
17. S. A. Thorpe (1982) On the Clouds of Bubbles Formed by Breaking Wind-waves in Deep Water, and Their Role in Air-sea Gas Transfer. *Philosophical Transactions of the Royal Society of London*, Series A, 304-155-210.
18. J. Smith (1998) Evolution of Langmuir circulation during a storm, *J. Geophys. Res.*, v103, C6, 12,649 - 12, 668.

19. D.M Farmer, S. Vagle, A. D. Booth (1998) A Free Flooding Acoustical Resonator for Measurement of Bubble Size Distributions, *J. Atmos. & Oceanic Technol.*, Vol. 15, No. 5, 1132-1146.
20. M. V. Trevorrow (1995) Measurement of Ocean Wave Directional Spectra Using Doppler Side-Scan Sonar Arrays, *J. Atmos. & Oceanic Technol.*, Vol 12, No. 3, 603-616.
21. G.B. Deane (1997) Sound Generation and Air Entrainment by Breaking Waves in the Surf Zone. *J. Acoust. Soc. Amer.*, 102, 2671-2689.
22. M. Li, C. Garrett (1995) Is Langmuir circulation driven by surface waves or surface cooling?, *J. Phys. Oceanogr.*, Vol. 25, 64-76.